Journal of Neurochemistry

JOURNAL OF NEUROCHEMISTRY | 2016 | 139 | 659–675 doi: 10.1111/jnc.13840

ORIGINAL ARTICLE

Imaging mass spectrometry reveals loss of polyunsaturated cardiolipins in the cortical contusion, hippocampus, and thalamus after traumatic brain injury

Louis J. Sparvero,*,†,[1] Andrew A. Amoscato,*,†,[1] Arthur B. Fink,*,† Tamil Anthonymuthu,‡ Lee Ann New,‡ Patrick M. Kochanek,‡ Simon Watkins,§ Valerian E. Kagan*,† and Hulya Bayır*,†,‡

*Department of Environmental and Occupational Health, University of Pittsburgh, Pittsburgh, Pennsylvania, USA

†Center for Free Radical and Antioxidant Health, University of Pittsburgh, Pittsburgh, Pennsylvania, USA

‡Department of Critical Care Medicine, and Safar Center for Resuscitation Research, University of Pittsburgh, Pittsburgh, Pennsylvania, USA

§Department of Cell Biology, University of Pittsburgh, Pittsburgh, Pennsylvania, USA

Abstract

Traumatic brain injury (TBI) leads to changes in ion fluxes, alterations in mitochondrial function, and increased generation of reactive oxygen species, resulting in secondary tissue damage. Mitochondria play important signaling roles in coordination of multiple metabolic platforms in addition to their well-known role in bioenergetics. Mitochondrial signaling strongly depends on cardiolipin (CL), a mitochondria-specific structurally unusual anionic phospholipid containing four fatty acyl chains. While our previous reports indicated that CL is selectively oxidized and presents itself as a target for the redox therapy following TBI, the topography of changes of CL in the injured brain remained to be defined. Here, we present a matrix-assisted laser desorption/ionization imaging study which reports regio-specific changes in CL, in a controlled cortical impact model of TBI in rats. Matrix-assisted laser desorption/ionization imaging revealed that TBI caused early decreases in CL in the contusional cortex, ipsilateral hippocampus, and thalamus with the most highly unsaturated CL species being most susceptible to loss. Phosphatidylinositol was the only other lipid species that exhibited a significant decrease, albeit to a lesser extent than CL. Signals for other lipids remained unchanged. This is the first study evaluating the spatial distribution of CL loss after acute brain injury. We propose that the CL loss may constitute an upstream mechanism for CL-driven signaling in different brain regions as an early response mechanism and may also underlie the bioenergetic changes

Received March 18, 2016; revised manuscript received August 29, 2016; accepted August 30, 2016.

Address correspondence and reprint requests to Hülya Bayır, MD, Children's Hospital of Pittsburgh, 4401 Penn Avenue, Pittsburgh, PA 15224, USA. E-mail: bayihx@ccm.upmc.edu and Valerian E. Kagan, PhD, Bridgeside Point, 100 Technology Drive, Room 330, Pittsburgh, PA 15219-3130, USA. E-mail: kagan@pitt.edu

[1]These authors contributed equally to this work.

Abbreviations used: AA, arachidonic acid; BSA, bovine serum albumin; CCI, controlled cortical impact; CL, cardiolipin; CL-ox, cardiolipin oxidation; COX, cyclooxygenase; cyt c, cytochrome c; DHA, docosahexaenoic acid; DHB, 2,5-dihydroxybenzoic acid; EDC, 1-ethyl-3-[3-dimethylaminopropyl]carbodiimide hydrochloride; EPA, eicosapentaenoic acid; IHC, immunohistochemistry; IMM, inner mitochondrial membrane; IMS, imaging mass spectrometry; ITO, indium-tin oxide; LC-MS, liquid chromatography-mass spectrometry; LOX, lipoxygenase; MALDI, matrix-assisted laser desorption/ionization; MALDI-MS, MALDI mass spectrometry; MES, 2-(4-Morpholino) ethane sulfonic acid; mPTP, mitochondrial permeability transition pore; MS/MS, tandem mass spectrometry (fragmentation analysis); MUFA, monounsaturated fatty acids; OMM, outer mitochondrial membrane; PA, phosphatidic acid; PC, phosphatidylcholine; PE, phosphatidylethanolamine; PFA, paraformaldehyde; PI3K, phosphatidylinositol-3-kinase; PI, phosphatidylinositol; PLC, Phospholipase C; PUFA, polyunsaturated fatty acids; ROS, reactive oxygen species; SCI, spinal cord injury; SFA, saturated fatty acids; SM, sphingomyelin; TBI, traumatic brain injury; TIC, total ion current; TMCL, tetramyristoylcardiolipin; TOF, time-of-flight.

that occur in hippocampal, cortical, and thalamic mitochondria after TBI.

Keywords: cardiolipin, hippocampus, imaging mass spectrometry, lipids, thalamus, traumatic brain injury.
J. Neurochem. (2016) **139**, 659–675.

Acute brain injury from trauma affects more than 1.5 million people every year in the United States alone (Mussack *et al.* 2002; Faul *et al.* 2010; Centers for Disease Control and Prevention 2013). Progress in management of critically ill neurological patients has led to improved survival rates after traumatic brain injury (TBI); however, only ~ 40% of patients sustaining severe TBI will attain either moderate or good recovery in their long-term follow-up (Mussack *et al.* 2002; Faul *et al.* 2010; Centers for Disease Control and Prevention 2013). The lifelong cost for continued care of a moderately to severely disabled person can exceed millions of dollars (Mussack *et al.* 2002; Faul *et al.* 2010; Centers for Disease Control and Prevention 2013). Therapies that prevent morbidity improve neurological outcome and quality of life in victims of TBI that are desperately needed. Studies in experimental TBI revealed that the cortex, hippocampus, and thalamus are selectively vulnerable to injury (Colicos *et al.* 1996; Tang *et al.* 1997; Sato *et al.* 2001; Geddes *et al.* 2003). Previous studies reported alterations in the lipid profile as an important contributor to this vulnerability and the evolution of secondary damage in TBI (Lewen *et al.* 2000; Bazan 2006; Hall *et al.* 2010). Subsequent to this, other studies have provided essential information on the spatial distribution of the altered lipid profile in response to traumatic brain injury, blast injury, and ischemia/reperfusion injury (Hankin *et al.* 2011; Woods *et al.* 2013; Roux *et al.* 2016) using imaging mass spectrometry. However, while the above studies focused on changes in sphingolipids/ceramides, sulfatides, gangliosides, diacylglycerols, and phospholipids which included phosphatidylethanolamine (PE), phosphatidylinositol (PI), and phosphatidylcholine (PC), they did not evaluate the spatial distribution of cardiolipin (CL). This information is important for the design and development of targeted therapies and evaluating their efficacy in TBI.

TBI occurs as a consequence of a direct mechanical impact, causing the brain to move rapidly within the cranium leading to tissue injury. As a consequence of membrane rupture at the site of impact and its immediate environment, there emerges an imbalance in the ionic equilibrium on post-synaptic membranes altering fluxes of K^+, Na^+, and Ca^{2+} ions, complicated by the pre-synaptic release of neurotransmitters and disorganized metabolic responses that may last from minutes to days (Werner and Engelhard 2007; Prins *et al.* 2013). Changes in cerebral blood flow and intracranial pressure also contribute substantially to tissue damage from the initial trauma (Werner and Engelhard 2007; Prins *et al.* 2013). Ineffective attempts by ionic pumps to reinstate the ionic homeostasis lead to ATP depletion causing an energy crisis, thus demanding increased respiration rates, resulting in elevated rates of electron flow through mitochondrial complexes (Werner and Engelhard 2007; Prins *et al.* 2013). This leads to increased production of reactive oxygen species contributing to further damage within mitochondria (Werner and Engelhard 2007; Cheng *et al.* 2012; Prins *et al.* 2013).

Similar imbalances in ionic equilibrium, mitochondrial dysfunction, and oxidative damage have been reported after cerebral ischemia (Bazan 1992; Chen *et al.* 2011) and traumatic injury to spinal cord (Azbill *et al.* 1997; Obrenovitch and Urenjak 1997; Stys and Li 1999; Sullivan *et al.* 2007). Indeed, reactive oxygen species (ROS), such as peroxynitrite and reactive aldehydes derived from the peroxidation of lipids, have been shown to be involved in the mitochondrial dysfunction associated with spinal cord injury and TBI (Xiong and Hall 2009; Vaishnav *et al.* 2010). As a result, numerous studies have demonstrated varying degrees of mitochondrial protection by scavenging lipid peroxyl radicals or using a variety of antioxidants and mitochondrial uncoupling agents (Mu *et al.* 2002; Jin *et al.* 2004; McEwen *et al.* 2007, 2011; Patel *et al.* 2009, 2010, 2012, 2014; Mustafa *et al.* 2010; Bains and Hall 2012).

In response to various forms of cellular insults which result in mitochondrial dysfunction, cells attempt to eliminate their depolarized and damaged mitochondria by employing a specialized type of autophagy, namely mitophagy – which, if successful, represents a rescue pathway (Kim and Lemasters 2011). Mitophagic signaling engages specialized lipid signaling whereby a unique mitochondrial phospholipid, cardiolipin (CL, Ptd_2Gro), gets translocated to the surface of the outer membranes and acts as an 'eat-me signal' (Chu *et al.* 2013). If mitophageal efforts are insufficient, the apoptotic program is activated to eradicate the cell. In this program, CL, more accurately its oxidation products, are involved as required executioners of the apoptotic program (Kagan *et al.* 2005). CL oxidation is catalyzed by an intermembrane space heme-protein, cytochrome c (cyt c). While cyt c normally acts as a shuttle of electrons between respiratory complexes III and IV, in depolarized mitochondria, it switches to become a CL-specific peroxidase thus contributing to the production of a variety of oxygenated lipid mediators (Kagan *et al.* 2005; Tyurina *et al.* 2014).

Thus, CLs are involved – as key signaling mechanisms – in responses of damaged neurons to mechanical trauma.

CLs (1,3-bis(sn-3′-phosphatidyl)-sn-glycerol) are structurally unusual anionic phospholipids as they contain two phosphatidyl groups (linked to a glycerol backbone) and four fatty acyl chains. In eukaryotic cells, mitochondrial CLs contain predominantly long carbon chains (from C16 to C22) that are polyunsaturated (from 2 to 6 double bonds). Importantly, these polyunsaturated fatty acids (PUFA) are readily oxidizable leading to the formation of numerous CL oxidation (CL-ox) products. CLs exist in low abundance compared to other phospholipids and are confined predominantly to the inner leaflet of the inner mitochondrial membrane, yet they play a central role in the life and death of cells. They associate with various components of the electron transport chain and are critical for overall mitochondrial bioenergetic function and are also partially responsible for maintaining mitochondrial architecture, giving the inner mitochondrial membrane its characteristic high degree of curvature (Hoch 1992; Schlame 2008; Kagan *et al.* 2009; Claypool and Koehler 2011; Osman *et al.* 2011; Rosca *et al.* 2011; Wirtz and Schuelke 2011; Winge 2012; Bazan *et al.* 2013). It is believed that these structural roles of CLs are fully met by the homoacylated species of CLs, such as tetralinoleoyl-CL, leading to its dominant presentation in mammalian tissues with high bioenergetic demands (e.g., heart, skeletal muscles) (Schlame *et al.* 1993). In contrast, high diversification is characteristic of tissues where the signaling functions of CLs are of critical importance culminating in more than 300 species in the brain (Bayir *et al.* 2007; Ji *et al.* 2012). This high degree of acyl chain diversification in CL was shown in an earlier report, whereby saturated fatty acids (SFAs), monounsaturated fatty acids, n-3 PUFAs, and n-6 PUFAs represented 20.2, 25.6, 23.5, and 30.7 mol % of the fatty acyl chain composition of total brain CL in the mice, respectively (Ellis *et al.* 2005). Interestingly, in mice lacking α-synuclein, CLs acyl chain composition was increased in SFA (51%) and decreased in n-6 PUFA (25%, Ellis *et al.* 2005). These changes were accompanied by a decrease in linked complex I/III electron transport chain (ETC) activity with no changes in individual complex activities noted. These results further support the importance of brain CL acyl chain diversity in bioenergetics and signaling in normal and pathological states.

While the diversity of CL species has been firmly established for the whole brain, surprisingly, the distribution and abundance of different CL species in different anatomical areas of the brain and their vulnerability to TBI-induced damage remain poorly characterized. This is mostly because of the low abundance of CL which is composed of multiple species. While our previous reports indicated that CL is selectively oxidized following TBI and presents itself as a target for the redox therapy of brain injury (Ji *et al.* 2012), the regional/spatial changes within damaged brain tissue with regard to this critical phospholipid remained undetermined. Here, we utilized our previously published protocol which employs a combination of enzymatic and chemical modifications on tissue in conjunction with matrix-assisted laser desorption/ionization (MALDI) mass spectrometry (Sparvero *et al.* 2010, 2012; Amoscato *et al.* 2014) to allow for successful mass spectrometric imaging of CL in brain tissue from a controlled cortical impact (CCI) TBI model. We demonstrate, for the first time, dramatic decreases in CL content in the contusional (cortical) area as well as in hippocampal and thalamic regions that are further removed from the site of injury.

Materials and methods

Reagents

Chloroform and ethanol (HPLC grade) were purchased from Sigma-Aldrich (St. Louis, MO, USA). Methanol was liquid chromatography-mass spectrometry (LC-MS) grade from Fisher Scientific (Pittsburgh, PA, USA). 2-(4-Morpholino)ethane sulfonic acid was BioReagent grade also from Fisher Scientific. Water was purified by a milliQ system (EMD Millipore, Billerica, MA, USA). 1-ethyl-3-[3-dimethylaminopropyl]carbodiimide hydrochloride (EDC) was purchased from Thermo Scientific/Pierce Biotechnology (Rockford, IL, USA). Phospholipase C (PLC) from *Bacillus cereus,* ammonium acetate, and 2,5-dihydroxybenzoic acid were also purchased from Sigma-Aldrich.

Animals and tissue preparation

All procedures were pre-approved and performed according to the protocols approved by the Institutional Animal Care and Use Committee of the University of Pittsburgh. TBI was induced by CCI to the left parietal cortex in three 17-day-old male Sprague–Dawley rats (Harlan, Indianapolis, IN, USA) as described previously (Ji *et al.* 2012). A metal pneumatically driven 6 mm impactor tip was used (impact velocity 4.0 ± 0.2 m/s, penetration depth 2.5 mm). Three naive 17-day-old male rats were used as controls. The brains were harvested 3 h after injury and immediately frozen in liquid nitrogen with neither fixation nor embedding, and stored at −80°C until sectioning. Brain tissue was affixed to a cryotome block with minimal Tissue-Tek OCT (Sakura FineTek USA, Torrance CA, USA). The blade and working surfaces of the cryotome were cleaned with methanol immediately prior to cutting, and at no time did the blade come into contact with the OCT. Six consecutive 10 μm coronal brain sections were cut at −21°C in the following order for: (i) MALDI-imaging mass spectrometry (IMS), (ii) H&E, (iii) MALDI-IMS, (iv) immunohistochemistry (IHC), (v) MALDI-IMS, (vi) lipid extraction. This sequence was repeated from Bregma −2.3 mm to Bregma −3.2 mm (Paxinos and Watson 1982). Sections for MALDI-IMS were applied to cold histology slides coated with a conductive indium-tin oxide surface (Delta Technologies LTD, Loveland, CO, USA), while other sections were applied to plain glass slides. This order allowed us to produce serial sections for ratiometric imaging of CL and semi-serial sections for H&E and the analysis of other lipid species. Lipid extraction from 5.0 mg of dried tissue sections on glass slides was performed using a modified Folch method as described previously (Folch *et al.* 1957). Total

lipid extracts were dried under a steady stream of grade 5.0 N_2, then dissolved in 2 : 1 chloroform : methanol to a total volume of 200 μL, and stored at −80°C prior to use.

For CL imaging, the tissue was prepared as previously described (Amoscato *et al.* 2014). Briefly, the tissue was first treated with 500 mM EDC in 2-(4-Morpholino)ethane sulfonic acid buffer (100 mM, pH 3.7) for 2 h at 24°C, then washed with 50 mM ammonium acetate buffer, pH 6.7 (200 μL per wash). The tissue was then treated with phospholipase C (0.005 units) for 15 min at 37°C in ammonium acetate buffer (50 mM, pH 6.7). The tissue was then washed again with ammonium acetate buffer as described above. After the chemical/enzymatic treatments, the tissue was vacuum dried (2 h). 2,5-dihydroxybenzoic acid solution (Sigma-Aldrich) was used as the matrix at 0.5 M in 2 : 1 chloroform : methanol with internal calibrants consisting of tetramyristoylcardiolipin and sphingomyelin (d18:1/12:0; Avanti Polar Lipids, Alabaster, AL, USA) at 5 and 20 μM, respectively. The matrix was applied using an aerosol device constructed in-house (Amoscato *et al.* 2014) and housed in a PCR chamber (Coy Laboratories, Grass Lake, MI, USA) inside a fume hood in order to minimize variability from airflow cross-currents. The nozzle height was 120 mm with a spray time of 10 min without interruption at a flow rate of 2400 μL/h.

Mass spectrometry analysis

MALDI time-of-flight – MS and IMS – analyses were performed using an ABI 4800 mass spectrometer equipped with an N_2 laser (AB Sciex, Framingham, MA, USA). Indium-tin oxide slides were fitted to the MALDI target with an AB 4800 Slide Glass Guide for two pieces (Hudson Surface Technology, Old Tappan, NJ, USA). All imaging was performed at a 200 μm lateral resolution with random walking every 50 laser shots. Using the instrument control software (AB Sciex), the laser attenuations value was set to 6100 arbitrary units. Three hundred shots were acquired per imaging location except for reflector-positive mode which used 100 shots. The mass analysis range was *m/z* 400–2000 in reflector-positive mode and 700–2000 in reflector-negative mode. For MS1 imaging, three tissue sections were imaged from each animal (two untreated analyzed with reflector-positive and -negative modes and one treated with EDC-PLC analyzed with reflector-negative mode). The negative-mode MS/MS imaging was performed on two additional EDC/PLC-treated sections from two out of the three animals and the mass windows were centered on the cardiolipin clusters at *m/z* 1448 (72-carbon CL) and 1476 (74-carbon CL) and was set at 20 Th to allow only species from that particular cluster. A grid of 200 μm coordinate locations covering the entire tissue section was generated on an Excel worksheet and imported into the MALDI control software as a custom plate type and spot set. Spatial locations for MALDI-IMS were determined by co-registering fiducials on optical images acquired from a microscope prior to matrix deposition. This spot set was run in batch mode to generate an array of t2d spectrum files. These files were converted to mzXML format using the t2d converter (downloaded from www.pepchem.org/download/converter.html) that uses OpenMS tools (Sturm *et al.* 2008). The data conversion requires Microsoft Windows 7 (www.microsoft.com) and Oracle Java (www.java.com). These mzXML files were then converted to mzML format with ProteoWizard (Chambers *et al.* 2012). A datacube in imzML format (Schramm *et al.* 2012) was then generated from these individual mzML files with imzML Converter (Race *et al.* 2012). Finally, the MALDI images were generated from the imzML datacube with MSI Reader v0.06 (Robichaud *et al.* 2013) using the following settings: total ion current (TIC) normalization, zero-order interpolation, intensity summing at 0.5 Da windows centered on the exact mass, jet heat map. For a detailed explanation regarding spectra acquisition and data conversion for td2 files on the ABI-4800 MALDI instrument, see Appendix S1.

MALDI-MS data analysis

Images are displayed as ion spatial distributions with intensities relative to the given ion (0% to 100% for all images). Using H&E-stained semi-serial sections and a rat brain atlas (Paxinos and Watson 1982) as a guide, areas around anatomical region of interest (ROIs) were drawn and the intensity information for given *m/z* values was exported into a spreadsheet using the 'ROI Selection' and 'Export Intensity Data' tools in MSI Reader. Since the size of the anatomical regions varied slightly between different animals, the total number of pixels from the ROIs for each animal varied. Average intensities of an ion within a given anatomical ROI were calculated and compared as ipsilateral/contralateral ratios (for CCI) or left/right ratios (for naive) from the same brain section. Each paired set of ion intensity ratios from a brain section's ROI was imported into its own spreadsheet. These ratios were compiled into naive and CCI-TBI groups. Three CCI animals and three naive animals were used for determining ratios and a two-tailed *t*-test was performed to determine significance of difference between these two groups for the ratios of the same ion. A one-way ANOVA (SPSS, IBM, Armonk, NY, USA) was performed to determine if a significant difference existed in CL loss between different molecular species within each CCI-TBI ROI. In order to determine which molecular species of CL showed significant differences in the amount of ipsi/contralateral loss as compared to other CL species, Tukey's *post hoc* test (SPSS, IBM) was performed between different molecular species within each CCI-TBI ROI.

Immunohistochemistry

The slides for IHC were stored at −20°C until they were ready to be stained. Sections were rehydrated with approximately 500 μL of phosphate-buffered saline (1× PBS). Chemical fixation in 2% paraformadehyde occurred at room temperature (19°C) for 20 min. The samples were then washed with approximately 1 mL of 1× PBS. Tissue permeabilization was accomplished via 0.1% Triton (Triton X-100, Cat. #: T-9184; Sigma, St Louis, MO, USA) detergent at 19°C for 15 min. Samples were washed with 1 mL of 0.5% bovine serum albumin (BSA) (bovine serum albumin lyophilized, Cat. #: A4503-50G; Sigma-Aldrich). Arbitrary binding of secondary antibodies was blocked using 20% normal goat serum (Sera from Normal Goat, Cat. #: G9023-5ML; Sigma-Aldrich) at 19°C for 45 min. Samples were washed with 1 mL of 0.5% BSA. Primary antibody, TOM20 (Host- Rabbit, Cat. #: sc-11415, working concentration 5 μg/mL; Santa Cruz Biotechnology, Santa Cruz, CA, USA) was diluted (1 : 100) in 0.5% BSA followed by incubation at 19°C for 1 h. The samples were then thoroughly washed with a volume of 3 mL of 0.5% BSA. Incubation with secondary antibodies goat-anti-mouse Cy3 (Cat. #: 115-165-166, working concentration 2 μg/mL; Jackson Immuno-Research, West Grove,

PA, USA) and goat-anti-rabbit Alexa Fluor 488 (Cat. #: A-11034, working concentration 2 μg/mL; Molecular Probes, Eugene, OR, USA) diluted (1 : 1000 and 1 : 500, respectively) in 0.5% BSA followed, at 19°C for 1 h. The samples were then thoroughly washed with a volume of 3 mL of 1× PBS. Hoechst nuclear stain (Cat. #: H3570, working concentration 10 μg/mL; Invitrogen, Carlsbad, CA, USA) was added to the samples and incubated at 19°C for 30–45 s. The samples were then washed with 1 mL of 1× PBS. Gelvatol mounting media was prepared according to a standard protocol (www.cbi.pitt.edu) and this was used to mount a cover glass to the slide.

Ratiometric imaging

Sections for ratiometric imaging were labeled with antibodies to TOM 20 (cat. # sc-11415/A3113; Santa Cruz Biotechnology, Inc., Dallas, TX, USA), nuclei counter-stained with Hoescht dye, and mounted as previously described (Amoscato *et al.* 2014). Entire sections were scanned and images were collected using a Nikon 90i (Melville, NY, USA) upright microscope, 20× dry plan apochromat objective, and motorized stage. Individual images were stitched together using Nikon Elements software. To overlay the MALDI-IMS data with the immunocytochemical data, fiduciary structures common to the semi-serial IMS and light microscopy images were identified. The MALDI-IMS images were resized such that the pixel count matched that of the light microscopy images and images combined into a single file. Various additive combinations of the MALDI-IMS images were made and rendered to the same bit depth (12 bit) as the light microscopy images and ratios calculated for MALDI-IMS intensity/mitochondrial label intensity. These images are displayed as monochrome images with a ratio between 0 and 50.

Statistical analysis

Data are expressed as mean ± SD as indicated in the figure legends. Changes in ipsi/contralateral signal intensities for given ion intensities for control and CCI tissue were analyzed by a two-tailed Student's *t*-test. In addition, CL ion intensities were analyzed by a one-way ANOVA (SPSS, IBM) and Tukey's *post hoc* test (SPSS, IBM) for comparisons. Differences were considered significant at $p < 0.05$.

Results

CL molecular species demonstrate regional specificity in the brain

Our MALDI imaging protocol resolved 23 isobaric species of CLs in the brain of control animals (Fig. 1a and b). The most abundant signals (CL species containing 72, 74, and 76 carbons) corresponded to CLs containing at least one or more arachidonic acid (AA) fatty acyl chain. A number of the CL clusters had intensities sufficient for fragmentation analysis indicating that the majority of the individual molecular forms were represented by PUFA-CLs, which were thus more abundant than non-oxidizable saturated and monounsaturated CLs [see Fig. 1b (top panel) and Table S1]. These MALDI data were independently confirmed by LC-MS/MS analysis (Fig. 1c). As in our MALDI-IMS analysis, our LC-MS analysis indicated a diverse speciation with the CL clusters containing 72 and 74 acyl carbons (CL 72:X, CL 74:X) as the prominent clusters (~ 25% each of total CL). This was followed by CL 76:X (~ 20%) and CL 70:X (~ 11%). Additional minor CL clusters accounted for the remaining percentage [78:X (~ 7%), CL 80:X (~ 7%), CL 68:X (~ 3%), not shown]. Our further detailed MS/MS fragmentation analysis indicated that all possible CL species (to approximately 94%) have at least one or more PUFA in their structure which was in line with previously published data (see Table S1, Bayir *et al.* 2007; Ji *et al.* 2012; Amoscato *et al.* 2014). Interestingly, this was dissimilar to CLs in many other mammalian tissues where linoleic acid-containing CL species dominate (Schlame *et al.* 1993; Schlame 2008).

Furthermore, we comparatively analyzed the CL speciation in four different anatomical regions of the brain (Fig. 1b). Overall, we found that signal intensities corresponding to concentrations of some of the CL species varied in different anatomical areas of the brain. This resulted in different 'biochemical' maps of individual CLs for the respective areas [e.g., compare heat map of CL (70 : 4) to that of CL (76 : 12) in Fig. 1a]. This also was reflected in the intensities of MALDI signals for these respective species collected from representative areas from each anatomical region as shown in Fig. 1(b). For example, the signal intensity of the CL (70:4) species was highest in the hippocampal area as compared to the cortex and thalamus and is reflected in the accompanying heat maps. Moreover, these specific spectra displayed differences from the MALDI spectra collected from the entire brain. Figure 1(d) displays a naive H&E-stained optical image with enlargements of representative areas. In the context of TBI-induced oxidative stress, these data indicate that the areas with higher levels of PUFA-CLs may be more vulnerable to oxidative modifications.

TBI results in decreases in cardiolipin molecular species at the site of injury and in the hippocampal and thalamic regions of the brain

CLs were severely decreased in the ipsilateral (impacted) side of the brain as compared to the contralateral side. This was most evident in the tissue immediately below the impact region where all CL species are decreased (compare Figs 1a and 2a). Intensity ratios for the CCI (ipsilateral/contralateral) and naive (left/right) samples are shown in Table S2. Ratios approaching unity indicate no change between regions, whereas ratios less than unity indicate a decrease in CL intensity between these regions within the same tissue section.

Comparison of the intensity ratios from CCI tissue sections to naive tissue sections at the same Bregma showed that each of the CL species were significantly lower in the injured region assessed at 3 h post-injury (as compared to the identical contralateral region) and lower as compared to the

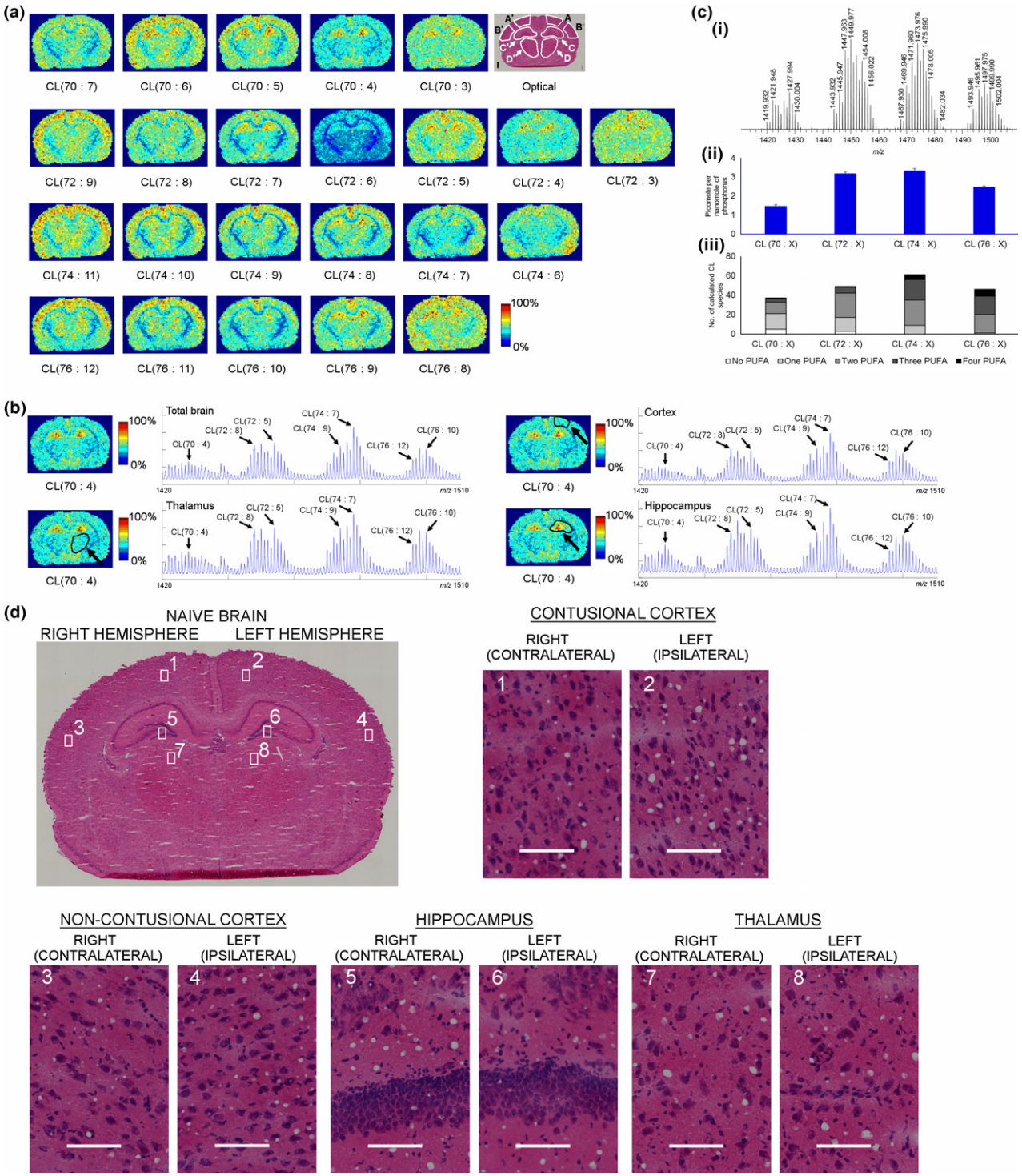

same CL species from the naive brain tissue sections ($p < 0.05$). Ranges for the CL ratios for the CCI versus naive contusional region (see Table S2) were as follows: CL, 70 carbon cluster, 0.78–0.81 versus 1.02–1.04; CL, 72 carbon cluster, 0.59–0.73 versus 1.08–1.10; CL, 74 carbon cluster, 0.46–0.60 versus 1.05–1.13; CL, 76 carbon cluster, 0.50–0.65 versus 1.07–1.1. We also noted a 'gradient' effect with regard to the CL species that were affected with the greater decreases associated with the more polyunsaturated CL species (Fig. 3a). This is clearly seen in the negative

Fig. 1 Matrix-assisted laser desorption/ionization mass spectrometry (MALDI-MS) images and representative spectra of cardiolipin (CL) in naive rat brain tissue (a): IMS negative ion mode heat maps of CL $[M-H]^-$ species from an entire naive rat brain coronal section (spatial resolution, 200 microns) treated with 1-ethyl-3-[3-dimethylaminopropyl]carbodiimide hydrochloride-PLC (representative images from three animals). Individual images for CL species include CL clusters 70:X, 72:X, 74:X, and 76:X indicating the total number of fatty acyl carbons (70, 72, 74, or 76) and the total number of double bonds (:X). A corresponding H&E optical image (scale bar = 1 mm) is shown with region of interest including (A,A') the left/right contusional region, (cortex); (B,B') an adjacent non-contusional region, (cortex); (C,C') the left/right hippocampus, and (D,D') the left/right thalamus, respectively. MALDI-MS images are displayed as relative intensities with respect to the given CL species. (b) Representative average CL $[M-H]^-$ spectra from total brain (intensity averaged from 2615 pixels), and ipsilateral thalamus (156 pixels), contusional cortex (89 pixels), and hippocampus (124 pixels). Representative heat maps for the CL (70:4) species for the different anatomical areas are shown as relative intensities with the region indicated. (c) (i) CL $[M-H]^-$ spectrum from liquid chromatography-mass spectrometry (LC-MS) analysis of rat brain cortex assessed within the same mass range as that presented for MALDI-IMS; (ii) quantitation of CL clusters; and (iii) a stacked histogram representing the number of possible CL species in each cluster containing zero, one, two, three, and four polyunsaturated fatty acids in their acyl chains. (d) H&E 4× optical image with zoom-in of representative regions at 10× including (1,2) right/left contusional cortex; (3,4) right/left non-contusional cortex; (5,6) right/left hippocampus; and (7,8) right/left thalamus, respectively. White scale bar = 100 microns.

slope associated with the ipsilateral side of the CCI cortex tissue (contusional) versus the near-zero slope of the adjacent (non-contusional) cortex (Fig. 4a and b).

We have extended our findings further to include ipsilateral/contralateral comparisons of three additional regions: (i) a cortical region adjacent to the area of impact; (ii) the hippocampus; and (iii) the thalamic region. Comparison of an adjacent cortical region to the area of impact to an identical contralateral region indicated that CL intensity ratios remained unchanged (i.e., ratios approaching unity, Figs 2a, 3b and Table S2). In addition, no significant CL changes were noted comparing this area to an identical area on a naive tissue section of the same Bregma (Table S2).

Interestingly, areas distant to the site of impact, such as the hippocampal and the thalamic regions, also suffered significant decreases ($p < 0.05$) in CL signals on the ipsilateral side as compared to the contralateral side (compare Figs 1a and 2a), although no histological evidence of damage was noted (Fig 2b). These results indicate that MSI is able to detect early CL alterations when histology cannot. Comparing the hippocampal CL ratios for the CCI versus naive tissue sections, the ranges (Table S2) were as follows: CL, 70 carbon cluster, 0.86–0.88 versus 1.00–1.01; CL, 72 carbon cluster, 0.75–0.88 versus 1.00–1.05; CL, 74 carbon cluster, 0.65–0.79 versus 1.00–1.05; CL, 76 carbon cluster, 0.68–0.78 versus 1.00–1.03. Likewise, the decreases in thalamic CL ratios for the CCI versus naive tissue sections were all significant ($p < 0.05$) and yielded the following results: CL, 70 carbon cluster, 0.88–0.90 versus 0.98–1.00; CL, 72 carbon cluster, 0.83–0.87 versus 0.98–1.02; CL, 74 carbon cluster, 0.74–0.88 versus 0.98–1.00; CL, 76 carbon cluster, 0.70–0.80 versus 0.95–0.98 (Figs 1a, 2, and 3c and d). Here again, a 'gradient' effect was observed: polyunsaturated CLs were affected more severely than CLs containing saturated (SFA) and monounsaturated fatty acids in both the hippocampal and thalamic areas (Fig. 4c and d). A comparison of *p*-values for individual CL species in CCI tissue is shown in Figure S1.

The decreases seen in CL species on the ipsilateral side at the site of impact, in an adjacent cortical region as well as in the hippocampal and thalamic regions are further supported by MS/MS data on CL clusters (Fig. 5b and d). MS/MS analysis of the remaining 72:X and 74:X CL clusters on the ipsilateral side of the CCI tissue indicated, as expected, decreases in CL product ions which included 16:0 (*m/z* 255.2), 16:1 (*m/z* 253.2), 18:0 (*m/z* 283.2), 18:1 (*m/z* 281.2), 18:2 (*m/z* 279.2), 20:4 (*m/z* 303.2), 22:6 (*m/z* 327.2) fatty acyl chains as well as intermediate phosphatidic acid (*m/z* 719.5, 699.5, 697.5, and 695.5) and lysoPA-H_2O (*m/z* 439.2, 417.2, 415.2, and 389.2) fragment ions. These changes were not evident in the naive samples (Fig. 5a and c).

MALDI imaging results for other phospholipid species in the impact region, adjacent cortex, hippocampal, and thalamic regions

PI species (*m/z* 883.5 and 885.5) displayed a significant ($p < 0.05$) decrease in ipsilateral/contralateral ratios in CCI tissue sections at the point of impact (Fig. 6 and Table S2) similar to that described for CL (intensity ratio range for PI, 0.36–0.44 vs. 1.0–1.1). Naive tissue sections showed no such changes. A significant decrease ($p < 0.05$) was noted for PI species *m/z* 885.5 in the hippocampus (intensity ratio range for CCI vs. naive 0.72–0.83 vs. 0.96–1.05), while a significant decrease ($p < 0.05$) in PI *m/z* 883.5 species was noted in the thalamus (intensity ratio range for CCI vs. naive 0.85–0.91 vs. 0.98–1.03). Neither of these decreases were as robust as that seen for CLs. No significant changes in PI intensity were noted in regions adjacent to the area of impact.

The major sulfatide species (*m/z* 806.6, 888.6, and 906.6, Fig. 6 and Table S2), which are not normally abundant outside the white matter, displayed no noticeable changes (ipsilateral/contralateral) in the thalamic and hippocampal regions in the CCI tissue sections. The major gangliosides displayed only a decrease at the point of impact (Figure S2), with ipsilateral/contralateral ratios below unity in some of the tissue sections (see Table S2 for individual ipsilateral/contralateral ratios). No other noticeable changes were evident for ganglioside species in the hippocampal, thalamic, and adjacent cortex regions.

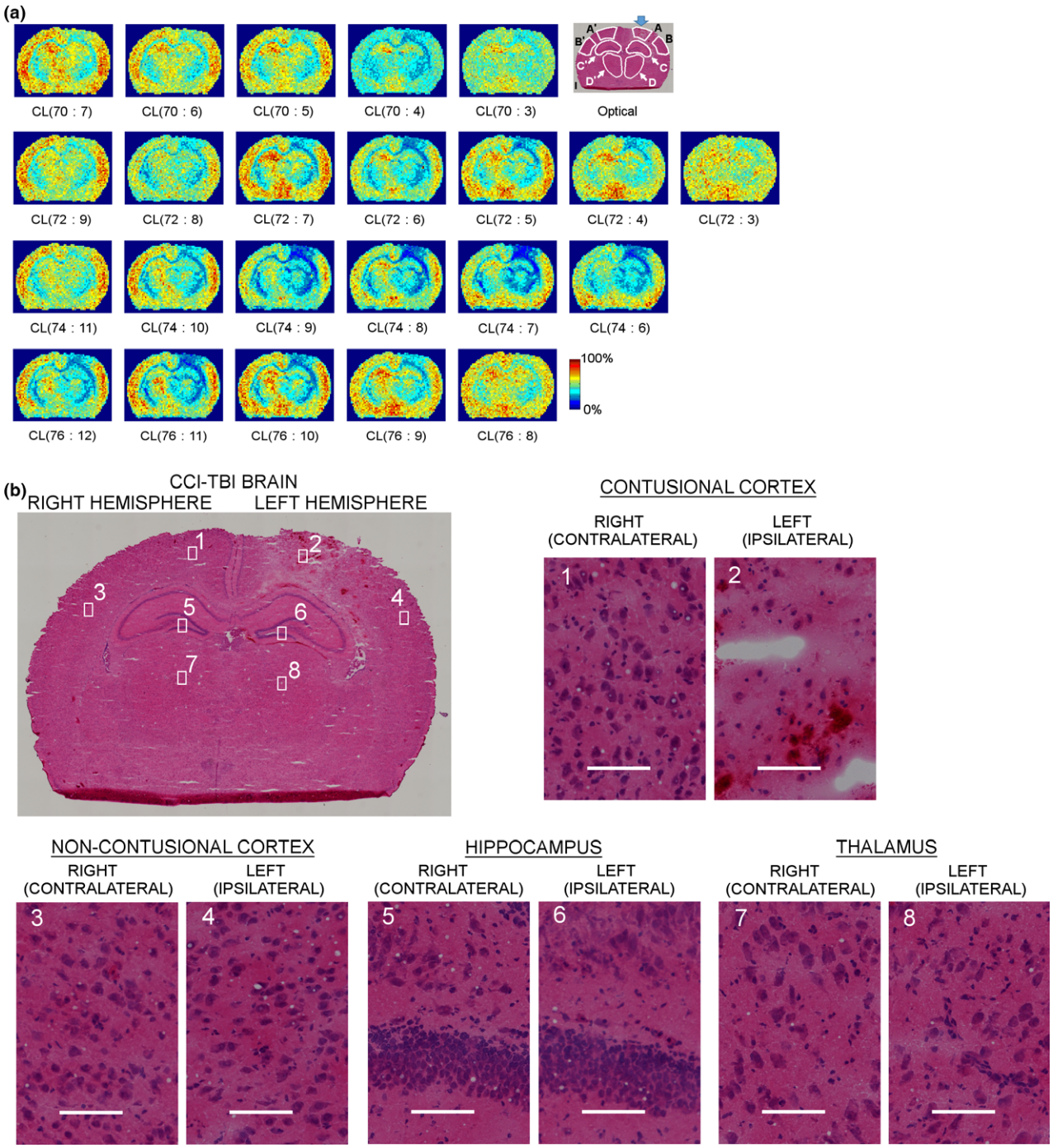

Fig. 2 Matrix-assisted laser desorption/ionization mass spectrometry (MALDI-MS) images of cardiolipin (CL) in controlled cortical impact (CCI) rat brain tissue (a). IMS negative ion mode heat maps of CL $[M-H]^-$ species from an entire CCI rat brain coronal section (spatial resolution, 200 microns) treated with 1-ethyl-3-[3-dimethylaminopropyl]carbodiimide hydrochloride-PLC (representative images from three animals). Individual images for CL species include CL clusters 70:X, 72:X, 74:X, and 76:X indicating the total number of fatty acyl carbons (70, 72, 74, or 76) and the total number of double bonds (:X). A corresponding H&E optical image (scale bar = 1 mm) is shown with regions of interest including (A,A') the ipsi/contralateral (right/left) contusional region, (cortex); (B,B') an adjacent non-contusional region, (cortex); (C,C') the ipsi/contralateral hippocampus; and (D,D') the ipsi/contralateral thalamus, respectively. The large blue arrow indicates the point of impact for the CCI tissue section. MALDI-MS images are displayed as relative intensities. (b) H&E 4× optical image with zoom-in of representative regions at 10× including (1,2) contra/ipsilateral contusional cortex; (3,4) contra/ipsilateral non-contusional cortex; (5,6) contra/ipsilateral hippocampus; and (7,8) contra/ipsilateral thalamus, respectively. White scale bar = 100 microns.

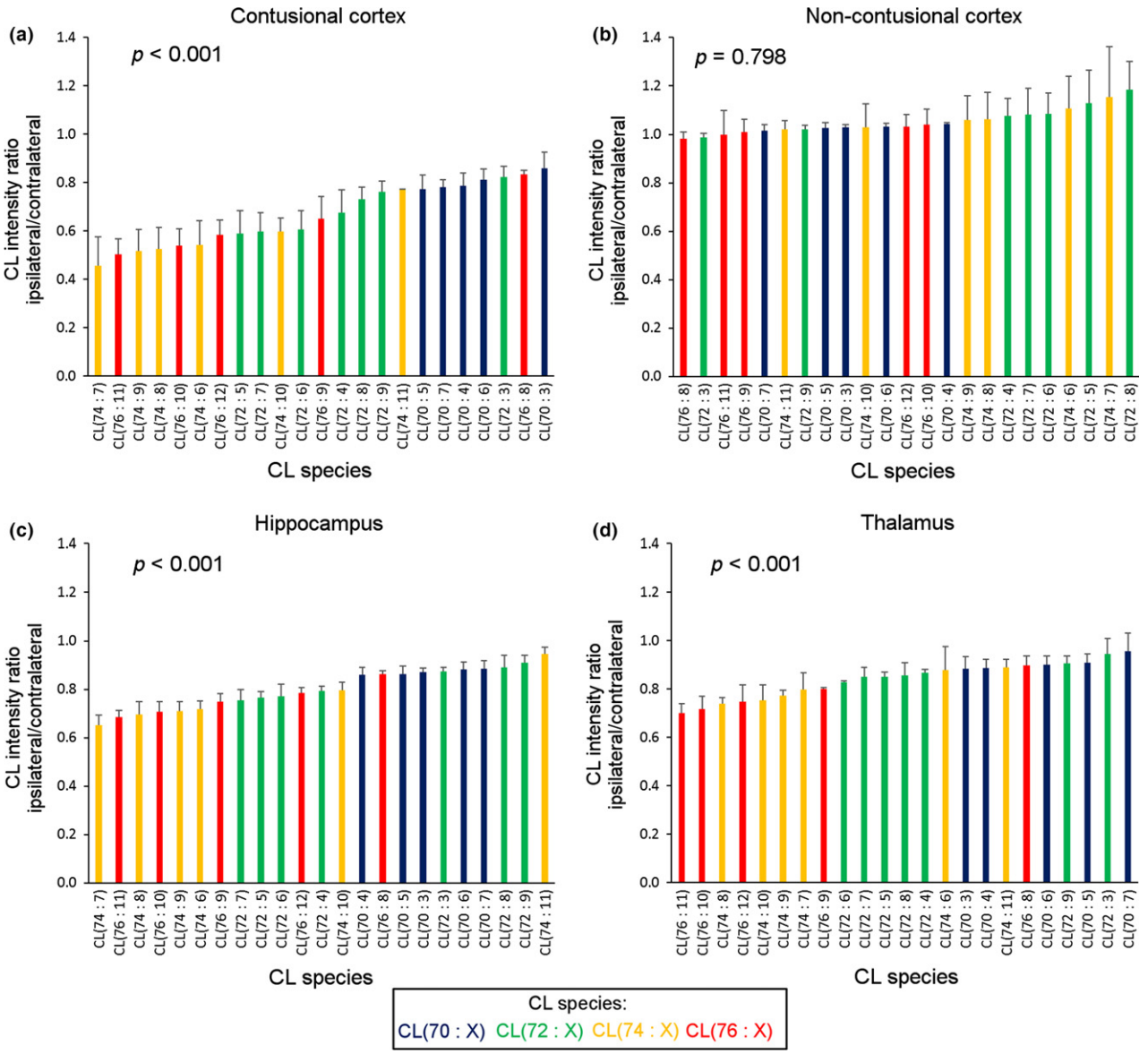

Fig. 3 Species-specific cardiolipin (CL) loss in the ipsilateral cortex, hippocampus, and thalamus in response to controlled cortical impact (CCI). Average CL signals from areas on the ipsilateral side of a CCI-traumatic brain injury section were divided by the average intensity of the same ion on an identical area on the contralateral side for the (a) contusional area (intensity averaged from 89 pixels per side), (b) an adjacent non-contusional area of the cortex (89 pixels), (c) hippocampus (124 pixels), and (d) thalamus (156 pixels). Ratios of CL signals were plotted for individual CL $[M\text{-}H]^-$ species ordered from the species most affected (i.e., greatest loss) to the species least affected (least loss). Ratios approaching unity indicate little to no loss. CL clusters containing 76 carbons (red), 74 carbons (yellow), 72 carbons (green), and 70 carbons (blue) are shown. One-way ANOVA determined that the between-groups *p*-value for different CL species was < 0.001 for each region of interest except for the non-contusional cortex.

Overall, these results indicate that the associated changes in intensities of the various lipids in the CCI model are not a generalized global effect on all lipids; rather, they are lipid and regio-specific. Moreover, CLs displayed the most pronounced TBI-induced regio-specific changes not only in the zone of immediate impact (cortex) but also in other anatomical areas – the hippocampal and thalamic ipsilateral regions of the brain.

Ratiometric analysis of CL to mitochondria confirms CL loss in the cortex contusional area as well as the hippocampus and thalamus

To confirm that the loss of CL signal in the CCI-TBI model was a result of insult rather than a change in the relative distribution of individual CLs in mitochondria among various anatomical areas of the brain, we performed ratiometric analysis of CL images relative to mitochondrial

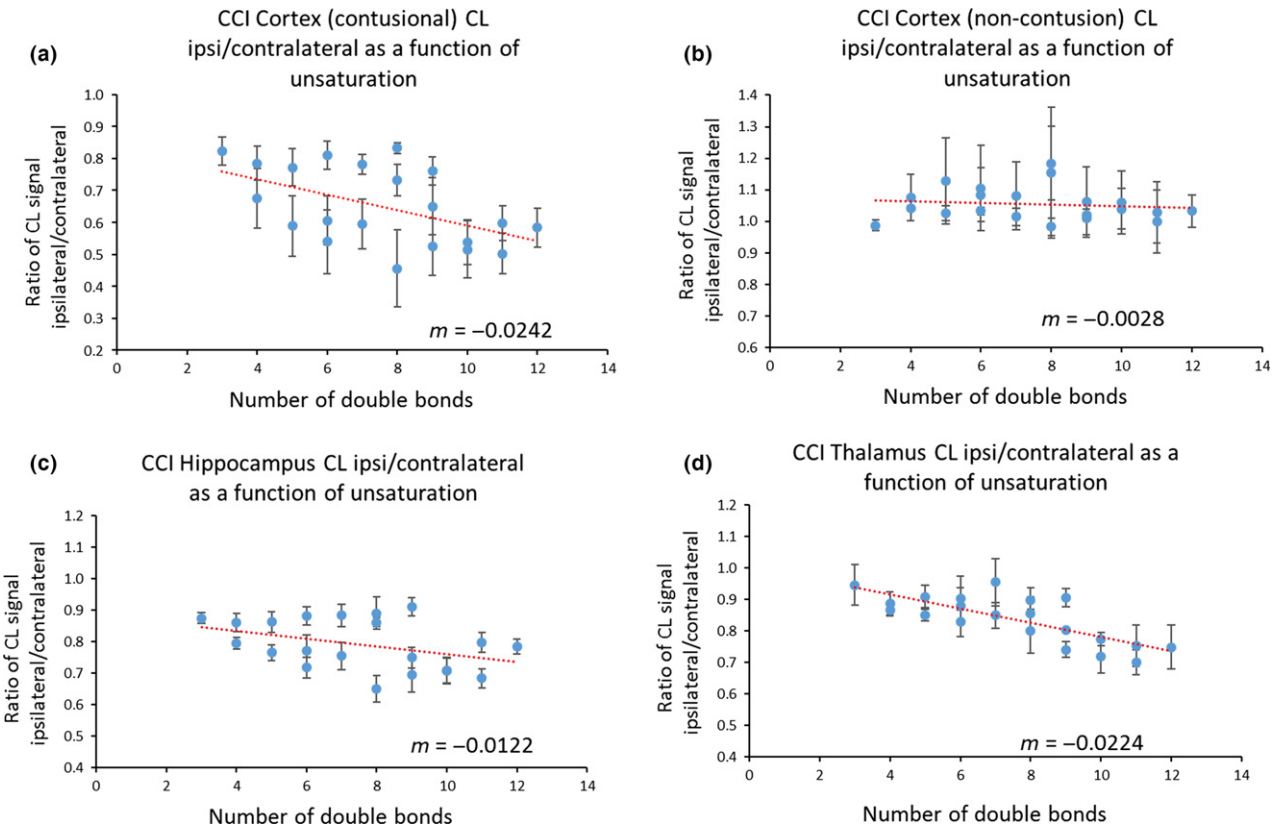

Fig. 4 Trend line analysis comparing the loss of cardiolipin (CL) signal in controlled cortical impact (CCI) tissue with the degree of CL unsaturation in various brain regions. Ipsilateral to contralateral ratios of CL signals were plotted versus number of double bonds contained in the CL species for the (a) cortex contusional area, (b) an adjacent non-contusional area of the cortex, (c) hippocampus, and (d) thalamus. A trend line was generated for each of the four brain areas above. Slopes (m) appear at the bottom of each graph. (a), (c), and (d) display negative slopes indicating a greater loss of CL signal with an increasing degree of unsaturation. Panel b displays little to no change.

abundance using immunohistochemical imaging of mitochondria from semi-serial sections. Ratiometric images in naive rat brain tissue correlated very well with our imaging mass spectrometry data, displaying little to no change in the cortex contusional area (a), a cortical region adjacent to the contusional area (b), the hippocampus (c), and thalamus (d) among the various CL species (Figure S3). In contrast, ratiometric images of CL in the CCI-TBI tissues displayed lower CL/mitochondrial ratios in the cortex contusional area (a), hippocampus (c), and thalamus (d), indicating less CL signal as compared to the mitochondrial IHC signal on the ipsilateral (damaged) side of the brain (Figure S4). CL/mitochondrial ratios on the contralateral side remained unchanged in these areas, confirming our finding that in the CCI-TBI model, CL loss extends into the hippocampal and thalamic areas on the ipsilateral side of the brain.

Discussion

This work presents, for the first time, a 'biochemical map' of individual molecular species of CLs and their distribution in several anatomical regions of normal and acutely injured brain. Two major mitochondrial functions of CLs: (i) structural in bioenergetics and (ii) signaling in coordinating metabolism – may be fulfilled by different molecular forms of CLs – homoacylated (mostly, tetralinoleoyl-CLs) and heteroacylated [CLs containing highly PUFA residues such as AA, eicosapentaenoic acid, docosahexaenoic acid (DHA)] (Schlame *et al.* 1993; Tyurina *et al.* 2014). The latter is achieved using CLs as a mitochondrial source of oxygenated lipid mediators generated via peroxidation of CLs by cyt c and subsequent hydrolysis of its oxidation products by Ca^{2+}-independent PLA_2 (Tyurina *et al.* 2014). This pathway is a Ca^{2+}-independent alternative to a conventional mechanism of the production of lipid mediators via the sequential action of Ca^{2+}-dependent PLA2 and oxygenation of the released free PUFA by lipoxygenase/cyclooxygenase-driven enzymatic reactions.

Acute brain injury, chronic neurodegenerative diseases, as well as spinal cord injury have been known to rely on lipid mediators, such as eicosanoids and docosanoids, as potent regulators of inflammatory responses. Eicosanoids generated

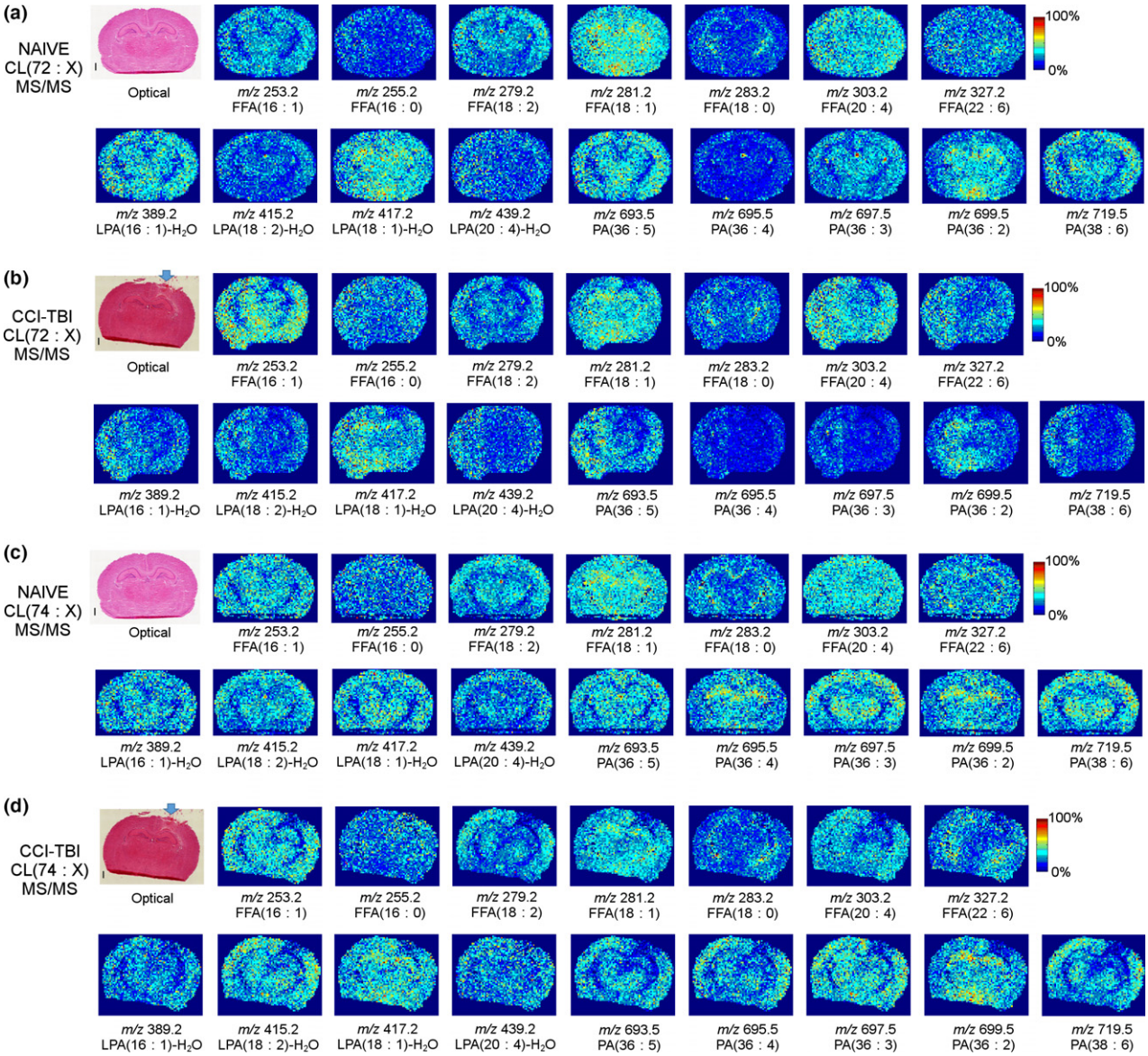

Fig. 5 Matrix-assisted laser desorption/ionization mass spectrometry (MALDI-MS) images of the cardiolipin (CL) (72:X) and (74:X) clusters in naive and controlled cortical impact (CCI)-traumatic brain injury (TBI) rat brain tissue. MS/MS analysis was performed on the CL cluster (72:X) centered around *m/z* 1448 for entire naive (a) and CCI-TBI (b) rat brain tissue coronal sections (representative images from two animals each, CCI and naive). A corresponding H&E optical image (scale bar = 1 mm) is shown for naive and CCI-TBI tissue. Heat maps for $[M-H]^-$ product ions of *m/z* 253.2, 255.2, 279.2, 281.2, 283.2, 303.2, 327.2, 415.2, 417.2, 693.5, 695.5, 697.5. 699.5, and 719.5 are shown which correspond to fatty acyl fragments 16:1, 16:0, 18:2, 18:1, 18:0, 20:4, 22:6, LPA (18:2)-H_2O, LPA (18:1)-H_2O, PA (36:5), PA (36:4), PA (36:3), PA (36:2), and PA (38:6), respectively. Spatial resolution = 200 microns. Arrow indicates the point of impact for the CCI tissue section. MALDI-MS images are displayed as relative intensities. MS/MS analysis was performed on the CL cluster (74:X) centered around *m/z* 1476 for entire naive (c) and CCI-TBI (d) rat brain tissue coronal sections. A corresponding H&E optical image (scale bar = 1 mm) is shown for naive and CCI-TBI tissue. Heat maps for fragments are the same as indicated above. Spatial resolution = 200 microns. Arrow indicates the point of impact for the CCI tissue section. MALDI-MS images are displayed as relative intensities.

through the enzymatic oxidation of AA via cyclooxygenases, lipoxygenases, and epoxygenases have potent effects on cell death, inflammation, and the immune response (Saunders *et al.* 1987; Murphy *et al.* 1994; Vane *et al.* 1998; O'Banion 1999; Kuhn and O'Donnell 2006; Phillis *et al.* 2006; Kim *et al.* 2008; Spector 2009). In particular, AA and DHA are released mainly by cytosolic phospholipase A_2 or plasmalogen-selective phospholipase A_2, respectively (Demediuk

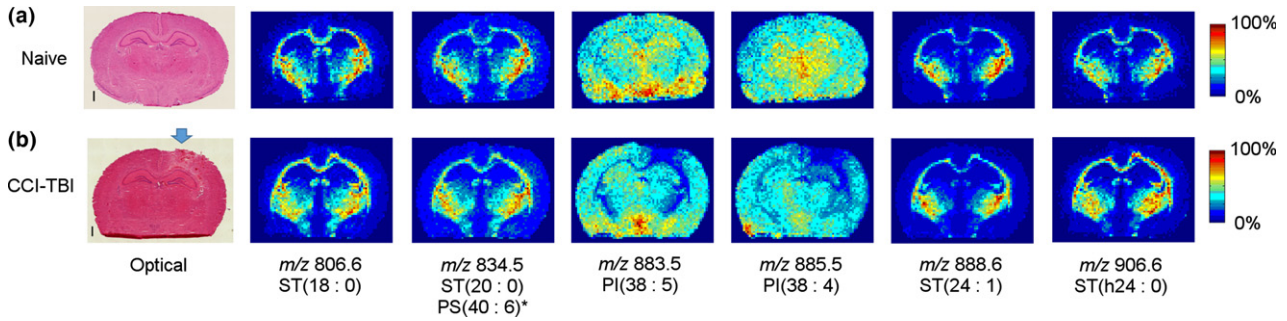

Fig. 6 Matrix-assisted laser desorption/ionization mass spectrometry (MALDI-MS) images of the major phosphatidylinositol (PI) and sulfatide species from rat brain tissue. Imaging mass spectrometry negative ion mode heat maps of the major PI and sulfatide species in naive (a) and controlled cortical impact (CCI)-traumatic brain injury (TBI) (b) rat brain tissue sections treated with 1-ethyl-3-[3-dimethylaminopropyl]carbodiimide hydrochloride-PLC (representative from three animals each, CCI and naive). A corresponding H&E optical image (scale bar = 1 mm) is shown for both naive and CCI-TBI tissue. Anionic lipid $[M\text{-}H]^-$ species include sulfatide (ST) 18:0, *m/z* 806.6; ST (20:0), *m/z* 834.5; ST (24:1), *m/z* 888.6; ST (24:0), *m/z* 906.6; PI (38:5), *m/z* 883.5; and PI (38:4), *m/z* 885.5. Arrow indicates the point of impact on the CCI tissue. *Indicates *m/z* 834.5 is isobaric with a PS (40:6) species. Spatial resolution = 200 microns. MALDI-MS images are displayed as relative intensities.

et al. 1985; Saunders *et al.* 1987; Hirashima *et al.* 1992; Farooqui *et al.* 2000; Farooqui 2010). Free AA is either incorporated into phospholipids by re-acylation or oxidized by enzymatic/non-enzymatic mechanisms producing a variety of signaling mediators involved in gene transcription, inflammation, oxidative stress, and neurodegeneration (Saunders *et al.* 1987; Murphy *et al.* 1994; Wolfe *et al.* 1994; Rapoport 1999; Farooqui *et al.* 2000; Lee *et al.* 2004;). On the other hand, DHA is converted into resolvins and neuroprotectins via 15-lipoxygenase-like enzymes (Hong *et al.* 2003; Marcheselli *et al.* 2003). While the mechanisms of formation of a variety of the AA and DHA precursors are known, their phospholipid precursors as well as the subcellular sites from which they originated (cytosolic vs. mitochondrial or other organelles) are less clear. With regard to this study, we report a loss of CL in the contusion which in part may be because of physical damage. In addition, we also suggest that, in the response to mechanical trauma, CL loss in the cortex and more importantly in the hippocampus and thalamus, may be a result of hydrolysis of various CL precursors for further downstream signaling events.

Traditionally, previous studies in the area of TBI have demonstrated a critical decrease in energy to the affected tissue, resulting in decreased amounts of ATP production allowing for an increased production of oxidative free radicals within mitochondria (Lifshitz *et al.* 2003, 2004; Robertson *et al.* 2004, 2006, 2007; Singh *et al.* 2006). The resulting energy crisis has been supported by subsequent studies demonstrating decreases in a variety of mitochondrial enzymatic activities which ultimately affect the overall structure and function of mitochondria.

Mitochondrial fate after TBI has been studied by several groups and their results paint a clear picture of mitochondrial biochemical demise. Robertson *et al.* (2004, 2006, 2007) reported a decrease in the pyruvate dehydrogenase complex activity as well as a decrease in cytochrome c content on the damaged (ipsilateral) side of rat brains at 4 h post-TBI in a CCI model. These findings were supported by other groups which demonstrated decreases in respiratory control ratios at 3 h post-TBI with subsequent increases in ROS and ultrastructural alterations in mitochondria which included swelling, disrupted cristae, and outer mitochondrial membrane rupture (Lifshitz *et al.* 2003, 2004; Robertson *et al.* 2007). As expected, less mitochondrial protein was present in the contusional area as compared to the corresponding contralateral area (Lifshitz *et al.* 2003, 2004). While the hippocampal mitochondrial protein levels remained unchanged between ipsilateral (impacted) and contralateral sides of the brain tissue, ATP levels declined significantly in the ipsilateral hippocampus (Lifshitz *et al.* 2003, 2004). A portion of these hippocampal mitochondria appeared to sustain damage, exhibiting swelling, ballooned membranes, and a reduced mitochondrial permeability transition pore sensitivity to Ca^{2+} (Lifshitz *et al.* 2003, 2004; Werner and Engelhard 2007; Prins *et al.* 2013). Indeed, many forms of TBI result in increased levels of Ca^{2+}, with excessive mitochondrial sequestration of this cation ultimately leading to the opening of the mitochondrial permeability transition pore, swelling and eventual outer mitochondrial membrane rupture and loss of cyt c (Robertson *et al.* 2004).

Since mechanical trauma has been associated with a decrease in ATP production, this will more than likely affect acyl chain turnover in the brain. Acyl-CoA-dependent remodeling is a highly energy-dependent process whereby approximately 25–30% of this tissue's energy expenditure is utilized for the maintenance of this biochemical process (Contreras *et al.* 2000; Rapoport 2001; Rapoport *et al.* 2002; DeMar *et al.* 2004; Igarashi *et al.* 2007; Lee *et al.* 2008;

Rapoport 2008). In addition to acyl chain turnover, increased energy expenditure may also be necessary for downstream lipid signaling (Bazan 2005; Chen and Bazan 2005; Lukiw and Bazan 2008). Indeed, energy expenditure is necessary for mitochondrial and cellular bioenergetics, metabolism, and signaling (Mitchell and Hatch 2009; Taylor and Harch 2009; Xu *et al.* 2010; Taylor *et al.* 2012; Mejia *et al.* 2014a,b, 2015; Mejia and Hatch 2016) which are comprised of a number of specific and irreversible chemical reactions. However, CL remodeling by tafazzin is both non-specific and reversible, producing only a minimal drop in free energy making this reaction essentially energy independent (Schlame *et al.* 1993, 2013). In addition, the literature indicates that the turnover of CL is slower than that of other phospholipids (Xu and Schlame 2014), such that substantial loss because of turnover within a 3 h post-CCI time period would be unlikely. Thus, the loss in CL as reported in this study may be the prelude to decreased ATP production, ultimately affecting overall lipid biosynthesis and remodeling at later time points.

Herein, we have described a mass spectrometric imaging study which investigated the changes in the critical mitochondrial phospholipid, CL, in a CCI model of TBI. With CL's intimate connection to mitochondrial bioenergetics, physiology, and structure, we provide evidence, for the first time, of regio-specific CL changes. Significant CL decreases occurred not only within the contusional area but also extended well beyond the area of impact into the hippocampus and thalamus following CCI. Phosphatidylinositol displayed significant decreases, although its changes in the hippocampal and thalamic regions were not as dramatic as compared to CL. Remarkably, signals for gangliosides, sulfatides, PC, and sphingomyelin (SM) remained essentially unchanged in the hippocampal and thalamic regions. Since our CL imaging protocol did not involve scanning in the *m/z* range below 400 to avoid potential low-mass matrix clusters and utilized PLC and EDC treatment of the tissue for CL visualization, we cannot rule out changes in cholesterol or plasmalogen species in response to TBI at later time points. Imaging of PC and SM lipids in positive mode provided two intriguing findings. First, sodium adducts of PC displayed an increase in the area of impact, whereas potassium adducts of the same PC species displayed a concomitant decrease (data not shown). The same held true for the SM species. These changes in the cortical impact area are in agreement with a previous study, whereby changes in PC adduct formation were noted in a mass spectrometric imaging study (Hankin *et al.* 2011). These findings most likely reflect neuronal depolarization and the resultant disrupted ionic equilibrium that occurs on the post-synaptic membranes in the contusional area, which drastically influences Na^+, K^+, and Ca^{2+} fluxes, likely causing a redistribution of lipid adduct ions.

Previous mass spectrometric imaging studies have provided essential information on the spatial distribution of various (non-cardiolipin) lipid species in response to blast injury and ischemia/reperfusion injury (Hankin *et al.* 2011; Woods *et al.* 2013). In the study assessing lipid changes in response to blast-induced 'mild' TBI, major increases in ganglioside GM2 were noted in the hippocampus, thalamus, and hypothalamus after a single blast exposure (Woods *et al.* 2013). Changes were seen as early as 2 h. On the other hand, a concomitant decrease in ceramides was also noted in the same study. Mass spectrometric imaging studies by Hankin *et al.* (2011) demonstrated changes in lysophosphatidylcholine, PC, PE, and SM that were specific to their adduct ions in response to ischemia/reperfusion injury in the brain. In an elegant study by Roux *et al.* (2016), the authors utilized an implanted silver nanoparticle protocol to image rat brain lipids over time in a CCI model of TBI. While CL was not assessed by this method and longer time points post-TBI were chosen (1, 3, and 7 days), their results indicated that increases in SM and ceramide were noted as early as 1 day post-TBI in the injured cortex. Their region of interest was defined by pixels that differed significantly from control when comparing the same lipid species. This region of interest included the cortical impact site and regions immediately adjacent to this. In addition, changes in diacylglycerols (increases in six species), cholesteryl esters (increases in eight species), PE (decreases in three species), PI (decrease/increase in one species), and sulfatides (decrease, one species) were noted at later time points (day 3 and 7 post-TBI). Thus, losses in CL at the 3-h time point as determined in this study may constitute an early response mechanism to TBI.

One possibility for the loss in CL and PI signals could be related to their potential for lipid oxidation in the presence of mitochondrial ROS generated following TBI because of the overall high degree of unsaturation present in their fatty acyl chains. This characteristic of CL and PI lipid species make them extremely susceptible to ROS attack and potential degradation. However, in this scenario, one would also expect other unsaturated lipid species to be prone to signal loss, however, this was not observed. While oxidation/degradation may contribute in part to loss of signal, cleavage of potential oxygenated PUFAs of CL, as potential mitochondrial lipid signals in response to TBI, may also be involved. Such a role for the generation of novel CL signals in mitochondria has already been reported in a cyt *c*/H_2O_2 model system (Tyurina *et al.* 2014). In this study, it was demonstrated that using brain CLs, a significant variety of lipid mediators could be generated by the cyt *c*-catalyzed oxygenation process. Specifically, eight well-known linoleic acid-based and nine AA-based lipid mediators were generated by cyt *c*/H_2O_2 from brain CLs. In a similar manner, PI loss (via head group modification and cleavage), having already been established as a traditional signaling cascade, may contribute to lower intensities of this lipid in the CCI model system. Indeed, several studies have demonstrated the

critical role of the phosphatidylinositol-3-kinase/Akt signaling pathway as a cell survival mechanism that is activated in the injured brain after TBI (Brazil *et al.* 2002; Iadecola and Anrather 2011; Chen *et al.* 2012). Thus, degradation of CL and PI via oxidation and specific cleavage of the oxidatively derived products functioning as upstream signaling molecules (either as damage sensors and/or as self-protective signals promoting neuronal survival) may both contribute to the overall loss of these lipid species as assessed by MS imaging in a CCI-TBI model system.

In conclusion, we have demonstrated, for the first time, regional/spatial CL decreases not only within the contusional area but also in the hippocampal and thalamic regions, distant from the site of injury in an established and well-characterized CCI model system of TBI. The decreases are not a generalized effect on all lipids; rather, they are confined predominantly to CL and PI. The specific decreases in CL, which ultimately will affect ETC function and mitochondrial architecture, are most likely key effectors of the decrease in various ETC enzymatic activities, the loss of cytochrome c, and the decrease in ATP production. While degradation of CL and PI via oxidation of their polyunsaturated fatty acyl chains by ROS may contribute to their subsequent loss, cleavage of these oxidized lipids as potential sources of lipid mediators should also be considered as an additional underlying mechanism that is activated as a self-protective/signaling response to traumatic brain injury. Future improved technologies will afford better resolved spatial resolution along with direct detection of oxygenated CL species and their signaling products.

Acknowledgments and conflict of interest disclosure

This work was supported by NIH: ES020693, U19AIO68021, NS076511, NS061817; NIOSH OH008282; U54 GM103529 08 (SCW); partial support from Fulbright Canada (VEK); WH81XWH-10-1-0623 and WH81XWH-14-2-0018 (PMK). This project used the UPCI Cancer Biomarkers Facility that is supported in part by award P30CA047904. The authors declare no competing financial interests.

All experiments were conducted in compliance with the ARRIVE guidelines.

Supporting information

Additional Supporting Information may be found online in the supporting information tab for this article:

Figure S1. Statistically significant differences between ipsilateral/contralateral ratios of different CL species in various CCI brain regions.

Figure S2. MALDI-MS images of the major ganglioside species from rat brain tissue.

Figure S3. Ratiometric images of CL in naïve rat brain tissue.

Figure S4. Ratiometric images of CL in CCI rat brain tissue.

Table S1. CL species identified in rat brain based on MS/MS fragmentation as determined from LC-MS analysis.

Table S2. Ipsilateral/contralateral intensity ratios for various lipid species.

Appendix S1. Spectra acquisition and data conversion for .t2d Files on the ABI-4800 MALDI for tissue imaging with full random walking.

References

Amoscato A. A., Sparvero L. J., He R. R., Watkins S., Bayir H. and Kagan V. E. (2014) Imaging mass spectrometry of diversified cardiolipin molecular species in the brain. *Anal. Chem.* **86**, 6587–6595.

Azbill R. D., Mu X., Bruce-Keller A. J., Mattson M. P. and Springer J. E. (1997) Impaired mitochondrial function, oxidative stress and altered antioxidant enzyme activities following traumatic spinal cord injury. *Brain Res.* **765**, 283–290.

Bains M. and Hall E. D. (2012) Antioxidant therapies in traumatic brain and spinal cord injury. *Biochim. Biophys. Acta* **1822**, 675–684.

Bayir H., Tyurin V. A., Tyurina Y. Y. *et al.* (2007) Selective early cardiolipin peroxidation after traumatic brain injury: an oxidative lipidomics analysis. *Ann. Neurol.* **62**, 154–169.

Bazan N. G. (1992) Modulators of neural cell signaling and triggering of gene expression following cerebral ischemia, in *Advances in Neurochemistry*, Vol. 7 (Ischen N. G., Braquet P. and Ginsberg M. D., eds.), pp. 321–333. Plenum Press, New York.

Bazan N. G. (2005) Lipid signaling in neural plasticity, brain repair and neuroprotection. *Mol. Neurobiol.* **32**, 89–103.

Bazan N. G. (2006) The onset of brain injury and neurodegeneration triggers the synthesis of docosanoid neuroprotective signaling. *Cell. Mol. Neurobiol.* **26**, 901–913.

Bazan S., Mileykovskaya E., Mallampalli V. K. P. S., Heacock P., Sparagna G. C. and Dowhan W. (2013) Cardiolipin-dependent reconstitution of respiratory supercomplexes from purified Saccharomyces cerevisiae complexes III and IV. *J. Biol. Chem.* **288**, 401–411.

Brazil D. P., Park J. and Hemmings B. A. (2002) PKB binding proteins. Getting in on the Akt. *Cell* **111**, 293–303.

Centers for Disease Control and Prevention. (2013) CDC grand rounds: reducing severe traumatic brain injury in the United States. *MMWR Morb. Mortal. Wkly Rep.* **62**, 549–552.

Chambers M. C., MacLean B., Burke R. *et al.* (2012) A cross-platform toolkit for mass spectrometry and proteomics. *Nat. Biotechnol.* **30**, 918–920.

Chen C. and Bazan N. G. (2005) Lipid signaling: sleep synaptic plasticity and neuroprotection. *Prostaglandins Other Lipid Mediat.* **77**, 65–76.

Chen H., Yoshioka H., Kim G. S., Jung J. E., Okami N., Sakata H., Maier C. M., Narasimhan P., Goeders C. E. and Chan P. H. (2011) Oxidative stress in ischemic brain damage: mechanisms of cell death and potential molecular targets for neuroprotection. *Antioxid. Redox Signal.* **14**, 1505–1517.

Chen S. F., Tsai H. J., Hung T. H., Chen C. C., Lee C. Y., Wu C. H., Wang P. Y. and Liao N. C. (2012) Salidroside improves behavioral and histological outcomes and reduces apoptosis via PI3K/Akt signaling after experimental traumatic brain injury. *PLoS ONE* **7**, e45763.

Cheng G., Kong R., Zhang L. and Zhang J. (2012) Mitochondria in traumatic brain injury and mitochondrial-targeted multipotential therapeutic strategies. *Br. J. Pharmacol.* **167**, 699–719.

Chu C. T., Ji J., Dagda R. K. *et al.* (2013) Cardiolipin externalization to the outer mitochondrial membrane acts as an elimination signal for mitophagy in neuronal cells. *Nat. Cell Biol.* **15**, 1197–1205.

Claypool S. M. and Koehler C. M. (2011) The complexity of cardiolipin in health and disease. *Trends Biomed. Sci.* **37**, 32–41.

Colicos M. A., Dixon C. E. and Dash P. K. (1996) Delayed, selective neuronal death following experimental cortical impact injury in rats: possible role in memory deficits. *Brain Res.* **739**, 111–119.

Contreras M. A., Greiner R. S., Chang M. C., Myers C. S., Salem N. and Rapoport S. I. (2000) Nutritional deprivation of alpha-linoleic acid decreases but does not abolish turnover and availability of unacylated docoahexaenoic acid and docosahexaenoyl-CoA in rat brain. *J. Neurochem.* **75**, 2392–2400.

DeMar J. C. Jr, Ma K., Bell J. M. and Rapoport S. I. (2004) Half-lives of docosahexaenoic acid in rat brain phospholipids are prolonged by 15 weeks of nutritional deprivation of n-3 polyunsaturated fatty acids. *J. Neurochem.* **91**, 1125–1137.

Demediuk P., Saunders R. D., Anderson D. K., Means E. D. and Horrocks L. A. (1985) Membrane lipid changes in laminectomized and traumatized cat spinal cord. *PNAS* **82**, 7071–7075.

Ellis C. E., Murphy E. J., Mitchell D. C., Golovko M. Y., Scaglia F., Barcelo-Coblijn G. C. and Nussbaum R. L. (2005) Mitochondrial lipid abnormality and electron transport chain impairment in mice lacking alpha-synuclein. *Mol. Cell. Biol.* **25**, 10190–10201.

Farooqui A. A. (2010) Studies on plasmalogen-selective PLA_2 in brain. *Mol. Neurobiol.* **41**, 267–273.

Farooqui A. A., Ong W. Y., Horrocks L. A. and Farooqui T. (2000) Brain cytosolic phospholipase A_2: localization, role and involvement in neurological diseases. *Neuroscientist* **6**, 169–180.

Faul M., Xu L., Wald M. M. and Coronado V. G. (2010) *Traumatic Brain Injury in the United States: Emergency Department Visits, Hospitalizations and Deaths 2002-2006*. Centers for Disease Control and Prevention, National Center for Injury Prevention and Control, Atlanta, GA.

Folch J., Lees M. and Sloane Stanley G. H. (1957) A simple method for the isolation and purification of total lipides from animal tissues. *J. Biol. Chem.* **226**, 497–509.

Geddes D. M., LaPlaca M. C. and Cargill R. S., 2nd (2003) Susceptibility of hippocampal neurons to mechanically induced injury. *Exp. Neurol.* **184**, 420–427.

Hall E. D., Vaishnav R. A. and Mustafa A. G. (2010) Antioxidant therapies for traumatic brain injury. *Neurotherapeutics* **7**, 51–61.

Hankin J. A., Farias S. E., Barkley R. M., Heidenreich K., Frey L. C., Hamazaki K., Kim H.-Y. and Murphy R. C. (2011) MALDI mass spectrometric imaging of lipids in rat brain injury models. *J. Am. Soc. Mass Spectrom.* **22**, 1014–1021.

Hirashima Y., Farooqui A. A., Mills J. S. and Horrocks L. A. (1992) Identification and purification of calcium-independent phospholipase A_2 from bovine brain cytosol. *J. Neurochem.* **59**, 708–714.

Hoch F. L. (1992) Cardiolipins and biomembrane function. *Biochim. Biophys. Acta* **1113**, 71–133.

Hong S., Gronert K., Devchaud P. R., Moussignac R. L. and Serhan C. N. (2003) Novel docosatrienes and 17S-resolvins generated from docoshexaenoic acid in murine brain, human blood, and glial cells-Autacoids in anti-inflammation. *J. Biol. Chem.* **278**, 14677–14687.

Iadecola C. and Anrather J. (2011) Stroke research at a crossroad: asking the brain for directions. *Nat. Neurosci.* **14**, 1363–1368.

Igarashi M., DeMar J. C. Jr, Ma K., Chang L., Bell J. M. and Rapoport S. I. (2007) Upregulated liver conversion of alpha-linolenic acid to docosahexaenoic acid in rats on a 15 week n-3 PUFA-deficient diet. *J. Lipid Res.* **48**, 152–164.

Ji J., Kline A. E., Amoscato A. *et al.* (2012) Lipidomics identifies cardiolipin oxidation as a mitochondrial target for redox therapy of brain injury. *Nat. Neruosci.* **15**, 1407–1413.

Jin Y., McEwen M. L., Nottingham S. A., Maragos W. F., Dragicevic N. B., Sullivan P. G. and Springer J. E. (2004) The mitochondrial uncoupling agent 2,4-dinitrophenol improves mitochondrial function, attenuates oxidative damage and increases white matter sparing in the contused spinal cord. *J. Neurotrauma* **21**, 1396–1404.

Kagan V. E., Tyurin V. A., Jiang J. *et al.* (2005) Cytochrome c acts as a cardiolipin oxygenase required for release of proapoptotic factors. *Nat. Chem. Biol.* **1**, 223–232.

Kagan V. E., Bayir H. A., Belikova N. A. *et al.* (2009) Cytochrome c/cardiolipin relations in mitochondria: a kiss of death. *Free Radic. Biol. Med.* **46**, 1439–1453.

Kim I. and Lemasters J. J. (2011) Mitophagy selectively degrades individual damaged mitochondria after photoirradiation. *Antioxid. Redox Signal.* **14**, 1919–1928.

Kim C., Kim J. Y. and Kim J. H. (2008) cytosolic phospholipase A2, lipoxygenase metabolites and reactive oxygen species. *BMB Rep.* **41**, 555–559.

Kuhn H. and O'Donnell V. B. (2006) Inflammation and immune regulation by 12/15-lipoxygenases. *Prog. Lipid Res.* **45**, 334–356.

Lee H., Villacreses N. E., Rapoport S. I. and Rosenberger T. A. (2004) In vivo imaging detects a transient increase in brain arachidonic acid metabolism: a potential marker of neuroinflammation. *J. Neurochem.* **91**, 936–945.

Lee H. J., Rao J. S., Chang L., Rapoport S. I. and Bazinet R. P. (2008) Chronic N-methyl-D-aspartate administration increases the turnover of arachidonic acid within brain phospholipids of the unanesthetized rat. *J. Lipid Res.* **49**, 162–168.

Lewen A., Matz P. and Chan P. H. (2000) Free radical pathways in CNS injury. *J. Neurotrauma* **17**, 871–890.

Lifshitz J., Friberg H., Neumar R. W., Raghupathi R., Welsh F. A., Janmey P., Saatman K. E. and Weiloch T. (2003) Structural and functional damage sustained by mitochondria after traumatic brain injury in the rat: evidence for differentially sensitive populations in the cortex and hippocampus. *J. Cereb. Blood Flow Metab.* **23**, 219–231.

Lifshitz J., Sullivan P. G., Hovda D. A., Weiloch T. and McIntosh T. K. (2004) Mitochondrial damage and dysfunction in traumatic brain injury. *Mitochondrion* **4**, 705–713.

Lukiw W. J. and Bazan N. G. (2008) Docosahexaenoic acid and the aging brain. *J. Nutr.* **138**, 2510–2514.

Marcheselli V. L., Hong S., Lukiw W. J. *et al.* (2003) Novel docosanoids inhibit brain ischemia-reperfusion-mdeiated leukocyte infiltration and pro-inflammatory gene expression. *J. Biol. Chem.* **278**, 43807–43817.

McEwen M. L., Sullivan P. G. and Springer J. E. (2007) Pretreatment with the cyclosporine derivative, NIM811, improves the function of synaptic mitochondria following spinal cord contusion in rats. *J. Neurotrauma* **24**, 613–624.

McEwen M. L., Sullivan P. G., Rabchevsky A. G. and Springer J. E. (2011) Targeting mitochondrial function for the treatment of acute spinal cord injury. *Neurotherapeutics* **8**, 168–179.

Mejia E. M. and Hatch G. M. (2016) Mitochondrial phospholipids: role in mitochondrial function. *J. Bioenerg. Biomembr.* **48**, 99–112.

Mejia E. M., Cole L. K. and Hatch G. M. (2014a) Mitochondrial metabolism and the role it plays in Heart failure and mitochondrial supercomplex formation. *Cadiovasc. Hematol. Disord. Drug Targets* **14**, 98–106.

Mejia E. M., Nguyen H. and Hatch G. M. (2014b) Mammalian cardiolipin biosynthesis. *Chem. Phys. Lipids* **179**, 11–16.

Mejia E. M., Ibdah J. A., Sparagna G. C. and Hatch G. M. (2015) Differention reduction in cardiac and liver monolysocardiolipin acyltransferase-1 and reduction in cardiac and liver tetralinoleoyl-cardiolipin in the alpha-subunit of trifunctional protein heterozygous knockout mice. *Biochem. J.* **47**, 123–129.

Mitchell R. W. and Hatch G. M. (2009) Regulation of cardiolipin biosynthesis by fatty acid transport protein-1 in HEK 293 cells. *Biochim. Biophys. Acta* **1788**, 2015–2021.

Mu X., Azbill R. D. and Springer J. E. (2002) NBQX treatment improves mitochondrial function and reduces oxidative events after spinal cord injury. *J. Neurotrauma* **19**, 917–927.

Murphy E. J., Behrmann D., Bates C. M. and Horrocks L. A. (1994) Lipid alterations following impact spinal cord injury in the rat. *Mol. Chem. Neuropathol.* **23**, 13–26.

Mussack T., Biberthaler P., Kanz K.-G., Wiedemann E., Gippner-Steppert C., Mutschler W. and Jochum M. (2002) Serum S-100B and interleukin-8 as predictive markers for comparative neurologic outcome analysis of patients after cardiac arrest and severe traumatic brain injury. *Crit. Care Med.* **30**, 2669–2674.

Mustafa A. G., Singh I. N., Wang J., Carrico K. M. and Hall E. D. (2010) Mitochondrial protection after traumatic brain injury by scavenging lipid peroxyl radicals. *J. Neurochem.* **114**, 271–280.

O'Banion M. K. (1999) Cyclooxygenase-2: molecular biology, pharmacology and neurobiology. *Crit. Rev. Neurobiol.* **13**, 45–82.

Obrenovitch T. P. and Urenjak J. (1997) Is high extracellular glutamate the key to excitotoxicity in traumatic brain injury? *J. Neurotrauma* **14**, 677–698.

Osman C., Velker D. R. and Langer T. (2011) Making heads or tails of phospholipids in mitochondria. *J. Cell Biol.* **192**, 7–16.

Patel S. P., Sullivan P. G., Pandya J. D. and Rabchevsky A. G. (2009) Differential effects of the mitochondrial uncoupling agent, 2,4-dinitrophenol, or the nitroxide antioxidant, Tempol, on synaptic or nonsynaptic mitochondria after spinal cord injury. *J. Neurosci. Res.* **87**, 130–140.

Patel S. P., Sullivan P. G., Lyttle T. S. and Rablchevsky A. G. (2010) Acetyl-L-carnitine ameliorates mitochondrial dysfunction following contusion spinal cord injury. *J. Neurochem.* **114**, 291–301.

Patel S. P., Sullivan P. G., Lyttle T. S., Magnuson D. S. and Rabchevsky A. G. (2012) Acetyl-L-carnitine treatment following spinal cord injury improves mitochondrial function correlated with remarkable tissue sparing and functional recovery. *Neuroscience* **210**, 296–307.

Patel S. P., Sullivan P. G., Pandya J. D., Goldstein G. A., VanRooyen J. L., Yonutas H. M., Eldahan K. C., Morehouse J., Magnuson D. S. and Rabchevsky A. G. (2014) N-acetylcysteine amide preserves mitochondrial bioenergetics and improves functional recovery following spinal trauma. *Exp. Neurol.* **257**, 95–105.

Paxinos G. and Watson C. (1982) *The Rat Brain in Sterotaxic Coordinates*. Academic Press, San Diego, California, USA.

Phillis J. W., Horrocks L. A. and Farooqui A. A. (2006) Cyclooxygenases, lipoxygenases and epoxygenases in CNS: their role and involvement in neurological disorders. *Brain Res. Rev.* **52**, 201–243.

Prins M., Greco T., Alexander D. and Giza C. C. (2013) The pathophysiology of traumatic brain injury. *Dis. Model. Mech.* **6**, 1307–1315.

Race A. M., Styles I. B. and Bunch J. (2012) Inclusive sharing of mass spectrometry imaging data requires a converter for all. *J. Proteomics.* **75**, 5111–5112.

Rapoport S. I. (1999) In vivo fatty acid incorporation into brain phospholipids in relation to signal transduction and membrane remodeling. *Neurochem. Res.* **24**, 1403–1415.

Rapoport S. I. (2001) In vivo fatty acid incorporation into brain phosholipids in relation to plasma availability, signal transduction and membrane remodeling. *J. Mol. Neurosci.* **16**, 243–261.

Rapoport S. I. (2008) Arachidonic acid and the brain. *J. Nutr.* **138**, 2515–2520.

Rapoport S. I., Chang M. C. and Spector A. A. (2002) Delivery and turnover of plasma derived essential PUFAs in mammalian brain. *J. Lipid Res.* **42**, 678–685.

Robertson C. L., Bucci C. J. and Fiskum G. (2004) Mitochondrial response to calcium in the developing brain. *Brain Res. Dev. Brain Res.* **151**, 141–148.

Robertson C. L., Soane L., Siegel Z. T. and Fiskum G. (2006) The potential role of mitochondria in pediatric traumatic brain injury. *Dev. Neurosci.* **28**, 432–446.

Robertson C. L., Saraswati M. and Fiskum G. (2007) Mitochondrial dysfunction early after traumatic brain injury in immature rats. *J. Neurochem.* **101**, 1248–1257.

Robichaud G., Garrard K. P., Barry J. A. and Muddiman D. C. (2013) MSiReader: an open-source interface to view and analyze high resolving power MS imaging files on matlab platform. *J. Am. Soc. Mass Spectrom.* **24**, 718–721.

Rosca M., Minkler P. and Hoppel C. L. (2011) Cardiac mitochondria in heart failure: normal cardiolipin profile and increased threonine phosphorylation of complex IV. *Biochim. Biophys. Acta* **1807**, 1373–1382.

Roux A., Muller L., Jackson S. N. *et al.* (2016) Mass spectrometry imaging of rat brain lipid profile changes over time following traumatic brain injury. *J. Neurosci. Methods* doi: 10.1016/j.jneumeth.2016.02.004. [Epub ahead of print]

Sato M., Chang E., Igarashi T. and Noble L. J. (2001) Neuronal injury and loss after traumatic brain injury: time course and regional variability. *Brain Res.* **917**, 45–54.

Saunders R. D., Dugan L. L., Demediuk P., Means E. D., Horrocks L. A. and Anderson D. K. (1987) Effects of methylprednisolone and the combination of alpha-tocopherol and selenium on arachidonic acid metabolism and lipid peroxidation in traumatized spinal cord tissue. *J. Neurochem.* **49**, 24–31.

Schlame M. (2008) Cardiolipin synthesis for the assembly of bacterial and mitochondrial membranes. *J. Lipid Res.* **49**, 1607–1620.

Schlame M. (2013) Cardiolipin remodeling and the function of tafazzin. *Biochim. Biophys. Acta* **1831**, 582–588.

Schlame M., Brody S. and Hostetler K. Y. (1993) Mitochondrial cardiolipin in diverse eukaryotes. *Eur. J. Biochem.* **212**, 727–733.

Schramm T., Hester A., Klinkert I. *et al.* (2012) imzML — A common data format for the flexible exchange and processing of mass spectrometry imaging data. *J. Proteomics.* **75**, 5106–5110.

Singh I. N., Sullivan P. G., Deng Y., Mbye L. H. and Hall E. D. (2006) Time course of post-traumatic mitochondrial oxidative damage and dysfunction in a mouse model of focal traumatic brain injury: implications for neuroprotective therapy. *J. Cereb. Blood Flow Metab.* **26**, 1–12.

Sparvero L. J., Amoscato A. A., Kochanek P. M., Pitt B. R., Kagan V. E. and Bayir H. (2010) Mass-spectrometry based oxidative lipidomics and lipid imaging: applications in traumatic brain injury. *J. Neurochem.* **115**, 1322–1336.

Sparvero L. J., Amoscato A. A., Dixon C. E., Long J. B., Kochanek P. M., Pitt B. R., Bayir H. and Kagan V. E. (2012) Mapping of phospholipids by MALDI imaging (MALDI-MSI): realities and expectations. *Chem. Phys. Lipids* **165**, 545–562.

Spector A. A. (2009) Arachidonic acid cytochrome P450 epoxygenase pathway. *J. Lipid Res.* **50**(Suppl), S52–S56.

Sturm M., Bertsch A., Gröpl C. *et al.* (2008) OpenMS – an open-source software framework for mass spectrometry. *BMC Bioinformatics* **9**, 163. doi:10.1186/1471-2105-9-163.

Stys P. K. and Li S. (1999) At physiological temperature, Na-Ca exchange plays an important role in mediating spinal cord white matter injury. *J. Neurotrauma* **16**, 984.

Sullivan P. G., Krishnamurthy S., Patel S. P., Pandya J. D. and Rabchevsky A. G. (2007) Temporal characterization of mitochondrial bioenergetics after spinal cord injury. *J. Neurotrauma* **24**, 991–999.

Tang Y. P., Noda Y., Hasegawa T. and Nabeshima T. (1997) A concussive-like brain injury model in mice (II): selective neuronal loss in the cortex and hippocampus. *J. Neurotrauma*, **14**, 863–873.

Taylor W. A. and Harch G. M. (2009) Identification of the human mitochondrial linoleoyl-Coenzyme A monolysocardiolipin acyltransferase (MLCL At-1). *J. Biol. Chem.* **284**, 30360–30371.

Taylor W. A., Majia E. M., Mitchell R. W., Choy P. C., Sparagna G. C. and Hatch G. M. (2012) Human trifunctional protein alpha links cardiolipin remodeling to beta-oxidation. *PLoS ONE* **7**, e48628.

Tyurina Y. Y., Poloyac S. M., Tyurin V. A. *et al.* (2014) A mitochondrial pathway for biosynthesis of lipid mediators. *Nat. Chem.* **26**, 1407–1418.

Vaishnav R. A., Singh I. N., Miller D. M. and Hall E. D. (2010) Lipid peroxidation-derived reactive aldehydes directly and differentially impair spinal cord and brain mitochondrial function. *J. Neurotrauma* **27**, 1311–1320.

Vane J. R., Bakhle Y. S. and Botting R. M. (1998) Cyclooxygenases 1 and 2. *Annu. Rev. Pharmacol. Toxicol.* **38**, 97–120.

Werner C. and Engelhard K. (2007) Pathophysiology of traumatic brain injury. *Br. J. Anaesth.* **99**, 4–9.

Winge D. R. (2012) Sealing the mitochondrial respirasome. *Mol. Cell. Biol.* **32**, 2647–2652.

Wirtz S. and Schuelke M. (2011) Region-specific expression of mitochondrial complex I genes during murine brain development. *PLoS ONE* **6**, 1–12.

Wolfe L.S. and Horrocks L.A. (1994) Eicosanoids in *Basic Neurochemistry* (Siegel G. L., Argranoff B. W., Albert R. W. and Molnoff P. B. eds), pp. 475–490. Raven Press, New York.

Woods A. S., Colsch B., Jackson S. N. *et al.* (2013) Gangliosides and ceramide change in a mouse model of blast induced traumatic brain injury. *ACS Chem. Neurosci.* **4**, 594–600.

Xiong Y. and Hall E. D. (2009) Pharmacological evidence for a role of peroxynitrite in the pathophysiology of spinal cord injury. *Exp. Neurol.* **216**, 105–114.

Xu Y. and Schlame M. (2014) The turnover of glycerol and acyl moieties of cardiolipin. *Chem. Phys. Lipids* **179**, 17–24.

Xu F. Y., McBride H., Acehan D., Vaz F. M., Houtkooper R. H., Lee R. M., Mowat M. A. and Hatch G. M. (2010) The dynamics of cardiolipin synthesis post-mitochondrial fusion. *Biochim. Biophys. Acta* **1798**, 1577–1585.